Handling power losses in a DC microgrid through constrained optimization

I. Zafeiratou, I. Prodan, F. Boem, L. Lefevre

Version of Record: https://www.sciencedirect.com/science/article/pii/S2405896320327853
Manuscript_56faaf9f6fa9e5600b1bc36759428718

Handling power losses in a DC microgrid through constrained optimization

I. Zafeiratou * **I. Prodan** * **F. Boem** ** **L. Lefèvre** *

* *Univ. Grenoble Alpes, Grenoble INP ⋆, LCIS, F-26000 Valence, France (e-mail: igyso.zafeiratou, ionela.prodan, laurent.lefevre@lcis.grenoble-inp.fr)*
** *University College London, London, UK (e-mail: f.boem@ucl.ac.uk)*

Abstract: This paper extends a hierarchical control approach for power balancing in a meshed DC microgrid while minimizing the power losses in the central transmission network. The control strategy is divided into three layers in hierarchical framework: i) the high level solves a continuous-time optimization problem which minimizes the DC-bus power loss and the electricity cost from the external grid power purchase through the combined use of differential flatness with B-splines parametrization; ii) the middle level employs a tracking Model Predictive Control (MPC) method which mitigates the discrepancies among the optimal and the actual profiles; iii) the low level controller handles the switching activity of the converters. The proposed approach is validated in simulation for a specific meshed DC microgrid system.

Keywords: DC microgrid, Power dissipation, Load balancing, Differential flatness, MPC

1. INTRODUCTION

Energy management and power distribution in microgrids play a major role and influence the power system operation. Power losses in the DC-bus network can significantly affect the power quality during transmission. Hence, their mitigation constitutes a very important factor for the power transmission improvement.

Different approaches have been proposed over the years for the power loss reduction, concentrating either on the components connected to the microrgid or on the central transmission network. Some works focus on topological issues or optimal scheduling of energy storage (ES) systems or renewable sources, as in Iovine et al. (2017). Nahata et al. (2019) propose a three-layer hierarchical control approach to solve the energy management problem in islanded microgrids. A two-level plug and play hierarchical controller was proposed in Vazquez et al. (2018).

This paper extends the hierarchical control scheme for a meshed DC microgrid in Zafeiratou et al. (2020) and concentrates on the minimization of power losses in the central transmission network (Fig. 1). The meshed DC microgrid and its components were already presented in Zafeiratou et al. (2020) (see also Fig. 1). In the high level, an optimization problem under constraints for power balancing and cost minimization was developed neglecting the power losses of the central transmission network. In here we concentrate on the high and middle levels proposing the following contributions: i) minimization of the power dissipation of the central transmission network is included in the optimization problem to optimize the power flow routing while minimizing the electricity cost; ii) detailed model description of the central power dissipation to represent the transmission lines including voltage drops among the connecting nodes [1] . Supplementary constraints are considered to maintain the voltage in the DC network close to 400 V; iii) validation of the approach through simulations considering different scenarios in the power losses among the sources and the loads.

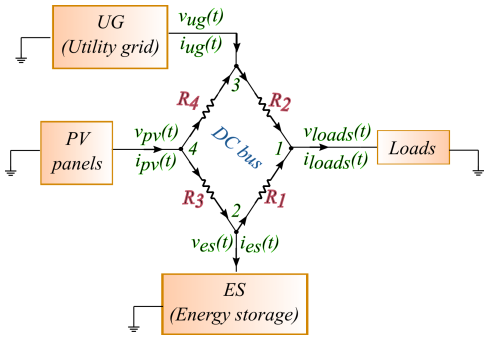

Fig. 1. Meshed DC microgrid architecture.

The cost function and the constraints will be written, through differential flatness [2] , in function of the B-splines to ensure continuous-time constraints validation.

2. MESHED DC MICROGRID ARCHITECTURE

This section will briefly present the ES model and will focus on the dynamics of the central transmission network. The hereinafter dynamics emerge from the port-

⋆ Institute of Engineering Univ. Grenoble Alpes

[1] A connecting node is the point where a source or a load is linked to the central network as in Fig. 1 for the nodes 1, 2, 3, 4.

[2] Differential flatness is a structural property of a class of nonlinear dynamical systems, denoting that all system variables (the states and the control inputs) can be written in terms of a set of specific variables, the so-called *flat outputs* (equal in number to the number of inputs), and their derivatives (Levine, 2009).

Hamiltonian (PH) modeling method which is detailed in Zafeiratou et al. (2020).

ES dynamical model: The ES system (Fig. 2) contains a lead acid battery connected to the Split-Pi converter. The state-space representation of the ES system is given in equations (4)-(7) in Zafeiratou et al. (2020) and will not be detailed here due to space limitation. Note that, from the ES circuit in Fig. 2, the battery's current is equal to $i_b(t) = i_{R_{1b}}(t)$ and the battery's voltage is equal to $v_b(t) = \frac{q_{1b}(t)}{C_{1b}}$, where $i_{R_{1b}}$ is the current of R_{1b} resistor, q_{1b} is the charge of C_{1b} capacitor and C_{1b} is its corresponding capacitance. These two relations will be used later in the control part. The duty cycles, $d_{1sc}(t)$ and $d_{2sc}(t)$, characterize the operation of the converter and are the control variables of the ES system, ($d_{1sc}(t)$ for switches Sw_{1sc} and Sw_{2sc} and $d_{2sc}(t)$ for switches Sw_{3sc} and Sw_{4sc}). The high-voltage DC-bus of the microgrid constrains the Split−Pi converter to always operate in down−conversion (towards the sources) and up-conversion (towards the central network) (Zafeiratou et al., 2020). Consequently, $d_{1sc}(t)$ will be always 0 and $d_{2sc}(t) \in (0, 1)$. Hence, let us denote in the following:

$$\alpha(t) = 1 - d_{2sc}(t), \tag{1}$$

which describes the relation between the two duty cycles in the Split-Pi converter.

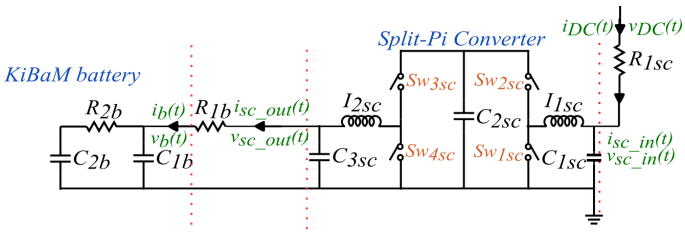

Fig. 2. Electrical circuit of ES.

Central transmission network: The transmission lines in this work are considered as resistors and, through the PH formalism, the network's model is described providing explicitly the relations of the voltages and currents on the connecting nodes [3] (see also Fig1):

- from node 1:

$$i_{loads} = i_{R_1} + i_{R_2} = \frac{v_{es} - v_{loads}}{R_1} + \frac{v_{ug} - v_{loads}}{R_2}, \tag{2a}$$

- from node 2:

$$i_{es} = i_{R_3} - i_{R_1} = \frac{v_{pv} - v_{es}}{R_3} - \frac{v_{es} - v_{loads}}{R_1}, \tag{2b}$$

- from node 3:

$$i_{ug} = i_{R_4} - i_{R_2} = \frac{v_{pv} - v_{ug}}{R_4} - \frac{v_{ug} - v_{loads}}{R_2}, \tag{2c}$$

- from node 4:

$$i_{pv} = i_{R_3} - i_{R_4} = \frac{v_{pv}(t) - v_{es}(t)}{R_3} - \frac{v_{ug}(t) - v_{pv}(t)}{R_4}. \tag{2d}$$

Because of the transmission-line power losses, there are deviations in the voltages on the connecting nodes. Hence, boundaries must be defined, which will maintain the voltages, $v_{ug}(t)$, $v_{pv}(t)$, $v_{es}(t)$, $v_{loads}(t)$, close to 400 V, as follows:

$$v_{DC}^{min,h} \leq v_{ug}(t),\ v_{pv}(t),\ v_{es}(t),\ v_{loads}(t) \leq v_{DC}^{max,h}. \tag{2}$$

Next, using (2a-2d), we express the power variables of the DC network as follows:

$$\begin{aligned} P_{ug} &= v_{ug} i_{ug} = v_{ug}[i_{R_4} - i_{R_2}] && \text{(3a)} \\ &= v_{ug}\left[\frac{v_{ug} - v_{pv}}{R_4} - \frac{v_{loads} - v_{ug}}{R_2}\right], \\ P_{es} &= v_{es} i_{es} = v_{es}[i_{R_3} - i_{R_1}] && \text{(3b)} \\ &= v_{es}\left[\frac{v_{pv} - v_{es}}{R_3} - \frac{v_{es} - v_{loads}}{R_1}\right], \\ P_{pv} &= v_{pv} i_{pv} = v_{pv}[i_{R_3} - i_{R_4}] && \text{(3c)} \\ &= v_{pv}\left[\frac{v_{pv} - v_{es}}{R_3} - \frac{v_{ug} - v_{pv}}{R_4}\right], \\ P_{loads} &= v_{loads} i_{loads} = v_{loads}[i_{R_1} - i_{R_2}] && \text{(3d)} \\ &= v_{loads}\left[\frac{v_{es} - v_{loads}}{R_1} - \frac{v_{loads} - v_{ug}}{R_2}\right], \end{aligned}$$

where P_{ug}, P_{es}, P_{pv}, P_{loads} are the electrical powers produced/consumed by the UG, ES, PV and loads components, respectively. The variables $v_{es}(t)$ and $i_{es}(t)$, $v_{pv}(t)$ and $i_{pv}(t)$, $v_{ug}(t)$ and $i_{ug}(t)$, $v_{loads}(t)$ and $i_{loads}(t)$ denote the input voltage and current on the connecting nodes of ES, PV, UG and loads components, respectively, as in Fig. 1. Next, the electrical power of the dissipative elements are also introduced:

$$P_{R_1} = \frac{[v_{es} - v_{loads}]^2}{R_1}, \tag{3e}$$

$$P_{R_2} = \frac{[v_{loads} - v_{ug}]^2}{R_2}, \tag{3g}$$

$$P_{R_3} = \frac{[v_{pv} - v_{es}]^2}{R_3}, \tag{3f}$$

$$P_{R_4} = \frac{[v_{ug} - v_{pv}]^2}{R_4}, \tag{3h}$$

where, P_{R_1}, P_{R_2}, P_{R_3}, P_{R_4} correspond to the power losses within the DC bus. In addition, the power conservation equation is presented below:

$$\begin{aligned} P_{ug}(t) + P_{pv}(t) - P_{es}(t) - P_{loads}(t) - P_{R1}(t) - \\ - P_{R2}(t) - P_{R3}(t) - P_{R4}(t) = 0. \end{aligned} \tag{4}$$

Flat representation of the ES: As mentioned in the Introduction we use differential flatness (Levine, 2009) since it allows us to make the connection between the nonlinear dynamics of the ES (Zafeiratou et al., 2020) and the forthcoming continuous-time constrained optimization problem for power balancing and power loss minimization. Therefore, the set of flat outputs together with the flat representation found for the ES system in Zafeiratou et al. (2020) are considered. Next, the B-spline parametrization is employed. Due to its properties (convexity, smoothness and differentiability), the continuous-time constraints validation can be verified (see also Prodan et al. (2019) and the references therein).

3. HIERARCHICAL CONTROL APPROACH

This section presents the extension of the three-level hierarchical control problem of the meshed DC microgrid including the power dissipation. Priority is given to the high and the middle level whose structure must be adapted appropriately to the dynamics of the central transmission network contrary to Zafeiratou et al. (2020). The three supervision levels consist of (see also the control scheme

[3] For compactness, whenever it is clear in the context, we discard the time dependence.

in Fig. 3): i) the high level, which generates optimal profiles not only for the power balancing, the current and the voltage of the battery, but also for the voltage on the connecting nodes and the duty cycle of the Split-Pi converter; ii) the middle level, where a tube-MPC contoller will track the optimal profiles obtained at the high level to minimize the discrepancies among the reference and the real profiles; iii) the low level, where the switching activity in the converter is validated (Zafeiratou et al., 2020).

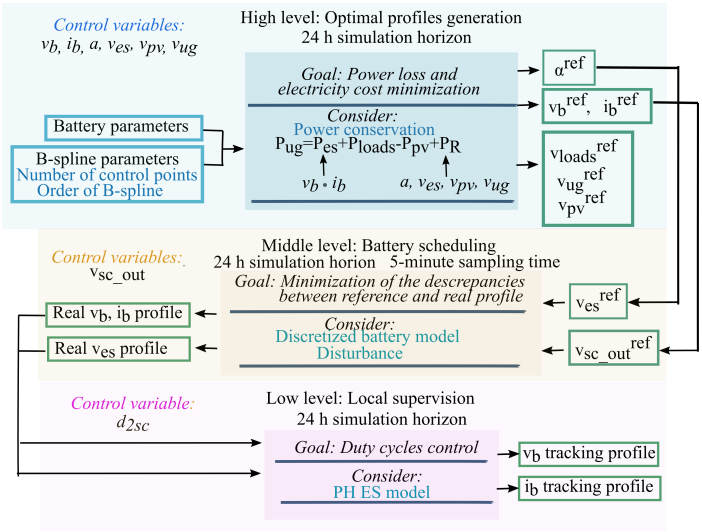

Fig. 3. Control scheme for the meshed DC microgrid.

3.1 High level problem formulation

Primary, the high level will be thoroughly analyzed. The objective function considered in Zafeiratou et al. (2020) was: $\min_{P_{ug}(t)} \int_{t_0}^{t_f} e(t)P_{ug}(t)dt$, where only the electricity cost was penalized neglecting power losses. Enhancing the previous work, we consider here the complete power conservation equation (4), where the P_{ug} is replaced by:

$$\begin{aligned} P_{ug}(t) =& P_{es}(t) + P_{loads}(t) - P_{pv}(t) + P_{R1}(t) + \\ &+ P_{R2}(t) + P_{R3}(t) + P_{R4}(t), \end{aligned} \tag{5}$$

including in this way the overall dynamics of the system. Consequently, the general objective function is [4]:

$$\begin{aligned} \min_{i_b, v_b, \alpha, v_{es}, v_{pv}, v_{ug}} \int_{t_0}^{t_f} e(t)\big[Q_{cost}\big(\underbrace{P_{es}(t)}_{i_b(t)v_b(t)}(t) + P_{loads}(t) - \\ - P_{pv}(t)\big) + Q_{loss}P_R(t)\big]dt, \end{aligned} \tag{6a}$$

$$subject\ to: \ system\ dynamics\ , \tag{6b}$$

$$power\ conservation\ (4), \tag{6c}$$

$$constraints\ for\ v_b\ ,\ i_b\ and\ q_{2b}\ , \tag{6d}$$

$$constraints\ for\ v_{ug},\ v_{pv},\ v_{es},\ v_{loads}\ (2), \tag{6e}$$

$$\begin{aligned} P_{ug}^{min,h} - P_{loads}(t) + P_{pv}(t) - P_R(t) \leq & P_{es}(t) \\ P_{es}(t) \leq P_{ug}^{max,h} + P_{loads}(t) - P_{pv}(t) - & P_R(t), \end{aligned} \tag{6f}$$

where $P_R(t) = P_{R1}(t) + P_{R2}(t) + P_{R3}(t) + P_{R4}(t)$ is the total power dissipation. In the following, we continue with the integration of the central dynamics in the optimization problem (objective function and constraints).

Note first that the converter is considered as an ideal element (power dissipation in the switches is neglected). Therefore, the input power, $P_{sc\_in}(t)$, is equal to the output power, $P_{sc\_out}(t)$ (Fig. 2):

$$P_{sc\_in}(t) = P_{sc\_out}(t) \tag{7a}$$

$$v_{sc\_in}(t)i_{sc\_in}(t) = v_{sc\_out}(t)i_{sc\_out}(t). \tag{7b}$$

Additionally, from the Ohm's law, we have:

$$v_{sc\_in}(t) = v_{es}(t) - R_{1sc}i_{es}(t) \tag{8a}$$

$$v_{sc\_out}(t) = v_b(t) + i_b(t)R_{1b} \tag{8b}$$

Combining the above equations (7) and (8) and considering that $i_{sc\_in}(t) = i_{es}(t)$ and $i_{sc\_out}(t) = i_b(t)$ lead to:

$$v_{es}(t) = \frac{v_b(t) + i_b(t)R_{1b}}{\alpha(t)} + R_{1sc}\alpha(t)i_b(t), \tag{9a}$$

$$i_{es}(t) = \alpha(t)i_b(t), \tag{9b}$$

where v_b and i_b are written in function of the flat outputs as presented in Zafeiratou et al. (2020). Therefore, from (9a) and (9b) the ES power and from (3e)-(3h) the P_R are deduced as follows:

$$\begin{aligned} P_{es}(t) =& v_{es}(t)i_{es}(t) = [v_b(t) + i_b(t)R_{1b}]i_b(t) + \\ &+ R_{1sc}[\alpha(t)i_b(t)]^2, \end{aligned} \tag{10a}$$

$$\begin{aligned} P_R(t) =& \Big(\frac{[v_{es}(t) - v_{loads}(t)]^2}{R_1} + \frac{[v_{loads}(t) - v_{ug}(t)]^2}{R_2} + \\ &+ \frac{[v_{ug}(t) - v_{pv}(t)]^2}{R_4} + \frac{[v_{pv}(t) - v_{es}(t)]^2}{R_3}\Big), \end{aligned} \tag{10b}$$

where $v_{es}(t)$, $i_{es}(t)$ are defined by (9a) and (9b) respectively. Additionally, some further restrictions are considered for the voltage of the loads, v_{loads}, the power generated by the PV, P_{pv}, and the power consumption, P_{loads}, as shown below (note that the voltage of the ES, v_{es}, is in function of the battery's dynamics as given above in (9a)):

$$\begin{aligned} from\ (2a):\ v_{loads}(t) = R_1 i_{es}(t) + (1 + \frac{R_1}{R_3})\cdot \\ \cdot v_{es}(t) - \frac{R_1}{R_3}v_{pv}(t), \end{aligned} \tag{11a}$$

$$\begin{aligned} from\ (3c):\ P_{pv}(t) = v_{pv}(t)i_{pv}(t) = v_{pv}(t)\cdot \\ \cdot \left[\frac{v_{pv}(t) - v_{es}(t)}{R_3} - \frac{v_{ug}(t) - v_{pv}(t)}{R_4}\right], \end{aligned} \tag{11b}$$

$$\begin{aligned} from\ (3d):\ \\ P_{loads}(t) - \epsilon_{loads} \leq v_{loads}(t)\left[\frac{v_{es}(t) - v_{loads}(t)}{R_1} - \right. \\ \left. - \frac{v_{loads}(t) - v_{ug}(t)}{R_2}\right] \leq P_{loads}(t) + \epsilon_{loads}, \end{aligned} \tag{11c}$$

where $\epsilon_{loads} \in \mathbb{R}$ makes (11c) a soft constraint, hence relaxing the load's demand to ensure the feasibility of the optimization problem in (6a)-(6f).

Two constraints remain for α and $P_{ug}(t)$ in (6f):

$$\frac{1}{\alpha(t)} > 1, \tag{12}$$

$$P_{ug}^{min,h} \leq P_{ug}(t) \leq P_{ug}^{max,h}, \tag{13}$$

To ensure constraint validation in continuous time, we consider (12) and (13) in function of the B-splines. In Zafeiratou et al. (2020) the flat outputs found for the battery are written in function of the B-splines.

[4] Note that (6b) and (6d) correspond to equations (4)-(7) and (15c)-(15e) respectively given in Zafeiratou et al. (2020).

Similarly to the flat outputs of the battery, we parametrize the α factor from (12) ($\frac{1}{\alpha(t)} \in (1, +\infty)$) using a set of B-splines, $\boldsymbol{b}_i$ of order d_α as follows:

$$\frac{1}{\alpha(t)} = \sum_{j=1}^{N_\alpha} \boldsymbol{p}_j^\alpha \boldsymbol{b}_{i,\boldsymbol{d}_\alpha}(t) \tag{14}$$

where N_α is the number of control points $\boldsymbol{p}_j^\alpha$, for which (according to B-splines properties) we deduce:

$$\boldsymbol{p}_j^\alpha > 1, \forall i = 1, \ldots, N_\alpha. \tag{15}$$

Next, for the constraint (13), we take into account (2c) and via (11a), (9a) and (9b), P_{ug} is rewritten as:

$$\begin{aligned} P_{ug}(t) =& v_{ug}^2(t)(\frac{1}{R_4} + \frac{1}{R_2}) + v_{ug}(t)v_{pv}(t)(\frac{R_1}{R_2R_3} - \frac{1}{R_4}) \\ &- \frac{1}{R_2}v_{ug}(t)\big[(1 + \frac{R_1}{R_3})\frac{v_b(t) + R_{1b}i_b(t)}{\alpha(t)} + \\ &+ (R_1 + R_{1sc} + \frac{R_1R_{1sc}}{R_3})\alpha(t)i_b(t)\big]. \end{aligned} \tag{16}$$

Therefore, the constraint (13) is defined as:

$$\begin{aligned} P_{ug}^{max,h} \geq& v_{ug}^2(t)(\frac{1}{R_4} + \frac{1}{R_2}) + v_{ug}(t)v_{pv}(t)(\frac{R_1}{R_2R_3} - \frac{1}{R_4}) \\ &- \frac{1}{R_2}v_{ug}(t)\big[(1 + \frac{R_1}{R_3})\frac{v_b(t) + R_{1b}i_b(t)}{\alpha(t)} - \\ &- (R_1 + R_{1sc} + \frac{R_1R_{1sc}}{R_3})|i_b(t)|\big], \end{aligned} \tag{17a}$$

$$\begin{aligned} P_{ug}^{min,h} \leq& v_{ug}^2(t)(\frac{1}{R_4} + \frac{1}{R_2}) + v_{ug}(t)v_{pv}(t)(\frac{R_1}{R_2R_3} - \frac{1}{R_4}) \\ &- \frac{1}{R_2}v_{ug}(t)\big[(1 + \frac{R_1}{R_3})\frac{v_b(t) + R_{1b}i_b(t)}{\alpha(t)} + \\ &+ (R_1 + R_{1sc} + \frac{R_1R_{1sc}}{R_3})|i_b(t)|\big], \end{aligned} \tag{17b}$$

which can be deduced also in function of the B-splines via $v_b(t)$ and $i_b(t)$. Hence, the optimization problem (6a)-(6f) is finally rewritten in function of the B-splines considering the constraints of the central transmission network as in (2), (11a)-(11c), (12)-(13). Next, the middle level is adjusted to the new considered dynamics with power losses included in the central transmission network. The reference profiles from the high level are: the battery current (i_b^{ref}), battery voltage (v_b^{ref}), input voltage of the ES (v_{es}^{ref}), output voltage ($v_{sc\_out}^{ref}$) and α factor (α^{ref}) of the Split-Pi converter.

3.2 Middle level

At this level, a tube-MPC controller tracks under perturbation the reference profiles obtained at the high level, minimizing the deviations among the reference and the real profiles. The discretized dynamical model of the battery will be considered (Zafeiratou et al., 2020). When considering the power losses, the MPC tracking problem is reformulated as follows:

$$\begin{aligned} \min_{\tilde{u}(k)} \sum_{i=k}^{k+N_p-1} & (\tilde{y}(i) - \tilde{y}^{ref}(i))^\top Q_{\tilde{y}}(\tilde{y}(i) - \tilde{y}^{ref}(i)) + \\ &+ (\tilde{u}(i) - \tilde{u}^{ref}(i))^\top R_{\tilde{u}}\left(\tilde{u}(i) - \tilde{u}^{ref}(i)\right) && \text{(18a)} \\ subject\ to: & \ the\ battery's\ discretized\ dynamics\ , && \text{(18b)} \\ & \tilde{v}_b^{min,m} \leq \tilde{v}_b(k) \leq \tilde{v}_b^{max,m}, && \text{(18c)} \\ & \tilde{i}_b^{min,m} \leq \tilde{i}_b(k) \leq \tilde{i}_b^{max,m}, && \text{(18d)} \\ & \tilde{v}_{es}^{min,m} \leq \tilde{v}_{es}(k) \leq \tilde{v}_{es}^{max,m}, && \text{(18e)} \\ & \tilde{P}_{ug}^{min,m} \leq \tilde{P}_{ug}(k) \leq \tilde{P}_{ug}^{max,m}, && \text{(18f)} \end{aligned}$$

with $\tilde{y}^{ref}(k) = \tilde{v}_{es}^{ref}(k)$ and $\tilde{u}^{ref}(k) = \tilde{v}_{sc\_out}^{ref}(k)$, taken at T_s sampling time. The last constraint $P_{ug}(t)$ is replaced by:

$$\begin{aligned} \tilde{P}_{ug}^{min,m} &- \tilde{P}_{loads}(k) + \tilde{P}_{pv}(k) - \tilde{P}_{R_1}(k) - \tilde{P}_{R_2}(k) - \\ &- \tilde{P}_{R_3}(k) - \tilde{P}_{R_4}(k) \leq \tilde{P}_{es}(k), \end{aligned} \tag{19a}$$

$$\begin{aligned} \tilde{P}_{ug}^{max,m} &- \tilde{P}_{loads}(k) + \tilde{P}_{pv}(k) - \tilde{P}_{R_1}(k) - \\ &- \tilde{P}_{R_2}(k) - \tilde{P}_{R_3}(k) - \tilde{P}_{R_4}(k) \geq \tilde{P}_{es}(k), \end{aligned} \tag{19b}$$

where $\tilde{P}_{es}(k) = \tilde{i}_{es}(k)\tilde{v}_{es}(k)$. The $\tilde{i}_{es}(k)$ and $\tilde{v}_{es}(k)$ are calculated with respect to the α factor reference profile α^{ref}, obtained at the high level and the equations (9a) and (9b) in discrete time.

4. SIMULATION AND COMPARISON RESULTS

In Table 1, the parameters of the DC microgrid are illustrated. Table 2 [5] depicts the parameters and constraints of the high and middle level controllers. The simulations are implemented in MATLAB 2015*a*. Furthermore, we use the YALMIP optimization toolbox for both high and middle level. This allows the use of IPOPT solver capable to handle nonlinear optimization problems.

Table 1. Parameters of the system.

Variable	Values	Units
R_{1sc}, R_{1b}, R_{2b}	1, 0.025, 0.088	$[\Omega]$
I_{1sc}, I_{2sc}	0.25, 0.25	$[H]$
C_{1sc}, C_{2sc}, C_{3sc}	0.0008, 0.0008, 0.0008	$[F]$
C_{1b}, C_{2b}	86400, 21600	$[F]$
R_1, R_2, R_3, R_4	1	$[\Omega]$

High level: In Fig. 4 the PV power and load profile are illustrated. The UG power and the ES power optimal profiles are generated through B-spline parametrization, with $N = 27$ and $N_\alpha = 18$ control points. The simulation is based on a constrained dynamics implementation in continuous−time over a horizon of 24 hours. In the figures, the red lines at the upper and lower level of each simulation represent the corresponding constraints (Table 2).

According to Fig. 4, the consumers' demand increases in the afternoon, while during the day until $3p.m.$ is more or less stable. Therefore, from $12p.m.$ to $12a.m.$, the *UG* and the *PV* charge the batteries. There is, also, a surpass of energy generated from the PV and it is sold to the UG (approximately 13% of the total power consumed). Furthermore, in Fig. 5, the battery's reference profiles for the current, voltage and charge are depicted as well as the α factor of the Split-Pi converter with the constraint verification. The electricity cost is equal to 2.713 euros.

[5] Note that N and d correspond to equations (17a)-(17b) given in Zafeiratou et al. (2020).

Table 2. Variables and constraints for the high and the middle level.

Level	Variable	Values	Units
High level	N	27	
	n_a as in (14)	18	
	d=d_a as in (14)	4	
	Q_{cost} as in (6a)	1	
	Q_{loss} as in (6a)	1	
Constraints	$v_b^{min,h}$, $v_b^{max,h}$	12, 13	$[V]$
	$i_b^{min,h}$, $i_b^{max,h}$	-9, 9	$[A]$
	$q_{2b}^{min,h}$, $q_{2b}^{max,h}$	72.5, 77.5	$[Ah]$
	$P_{ug}^{min,h}$, $P_{ug}^{max,h}$	-2100, 4200	$[W]$
	$v_{DC}^{min,h}$, $v_{DC}^{max,h}$	380, 420	$[V]$
Middle level	N_p as in (18a)	5	
	T_s	300	$[s]$
	$Q_{\tilde{y}}$ as in (18a)	$diag(1,1)$	
	$R_{\tilde{u}}$ as in (18a)	100	
Constraints	$v_b^{min,m}$, $v_b^{max,m}$	11.9, 13.1	$[V]$
	$i_b^{min,m}$, $i_b^{max,m}$	-10.6, 10.6	$[A]$
	$P_{ug}^{min,m}$, $P_{ug}^{max,m}$	-2100, 4200	$[W]$
	$v_{DC}^{min,h}$, $v_{DC}^{max,h}$	370, 430	$[V]$

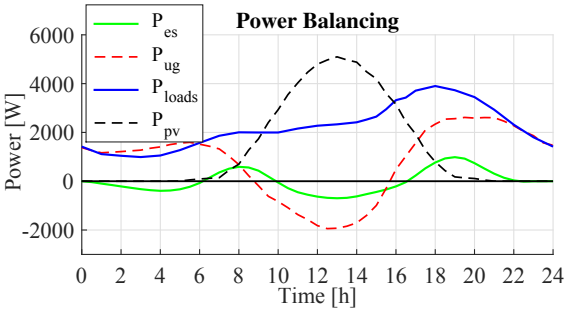

Fig. 4. Optimal power flow of the power sources.

Table 3. Power percentage with respect to the total power produced or consumed (high level).

Power	Power produced [%]	Power consumed [%]
P_{ug}	42.14%	13% sold to the UG
P_{es}	6.58%	6.7% for ES charging
P_{pv}	51.28%	-
P_{loads}	-	79.66% for load usage
P_{loss}	-	Total: 0.64% R_1: 0.12% R_2: 0.21% R_3: 0.13% R_4: 0.18%

Afterwards, the power losses are presented in Fig. 6 together with the constraint validation for the voltage on the four connecting nodes (Fig. 7) where the sources and the loads stand. The power losses in lines R_3 and R_4 are caused by the PV purchase towards the UG or the ES system. The total loss of R_1 and R_2, about 0.33%, exists due to the load demand that increases after $4p.m.$. The total calculation time of the simulation is around 12 m.

Middle level: As aforementioned, in the middle level, we use MPC for reference tracking with a prediction horizon

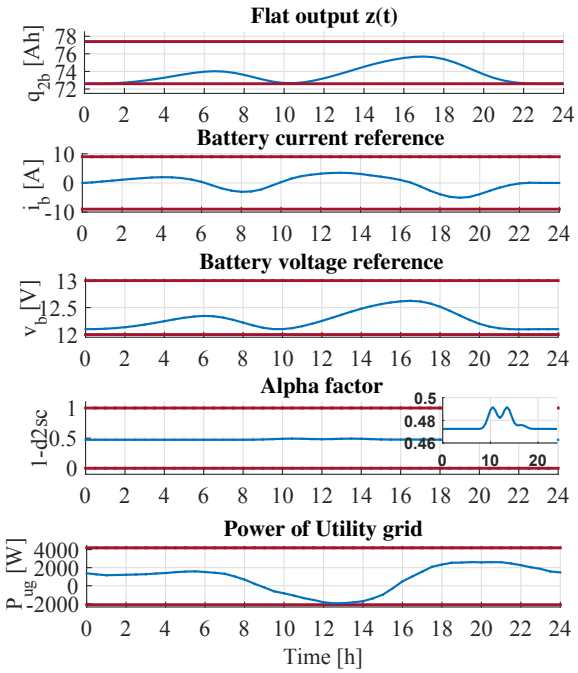

Fig. 5. Reference profiles of the high level.

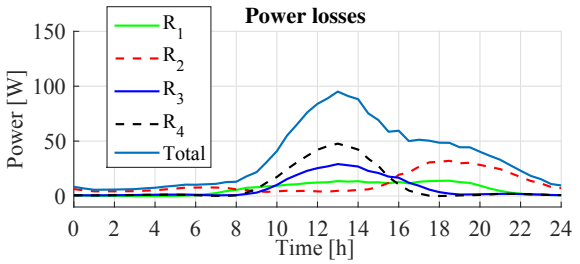

Fig. 6. Power losses in transmission lines.

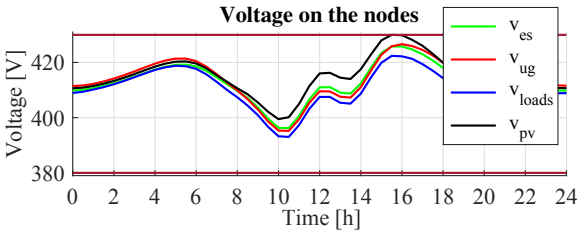

Fig. 7. Corresponding voltages on the nodes.

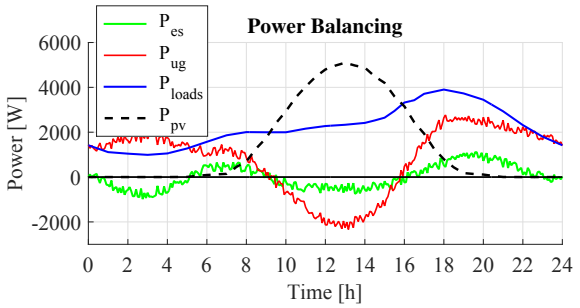

Fig. 8. Real power flow profiles of the power sources.

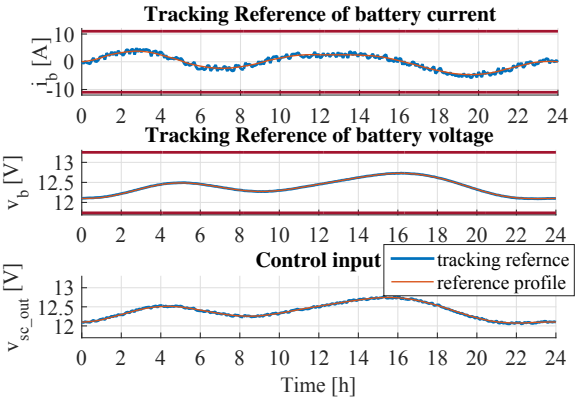

Fig. 9. Tracking profiles.

N_p equal to 5 and a sampling time T_s equal to 300 s. In Fig. 8, we observe the tracking profiles of the *Power Balancing*, and the control input, v_{sc_out} (the output voltage of the Split-Pi converter), which is in function of the current, i_b, and the voltage, v_b of the battery as in (8b). From the figures Fig. 8 and Fig. 9, we observe that the optimal profiles obtained at the high level are very closely followed.

Comparison with MPC for optimal profile generation: As a next step, we compare the reference trajectories generation at the high level (for R_1=R_2=R_3=R_4=1 Ω) obtained through differential flatness and B-spline parametrization with MPC method, used for instance in Velarde et al. (2017). Hence, we present the simulation results for the reference profiles obtained with the profiles obtained using MPC in Fig. 10 with a prediction horizon equal to 24 and a sampling time equal to 1200. Similar trajectories are observed with a slight difference in the cost as it is depicted also in Table 4 of about $0.3 - 3\%$. Furthermore, we observe that because of the dynamics discretization in MPC, the value of the sampling time influences the simulation's performance (note in particular the variation in the electricity cost).

Table 4. Simulation results obtained for optimal profiles with MPC.

Prediction horizon N_p	Sampling time T_s [s]	Electricity cost [euros]	Power loss [%]
24	1200	2.801	1.63%
15	1800	2.747	1.65%
10	1800	2.788	1.64%

5. CONCLUSION

The paper extends the method presented in Zafeiratou et al. (2020) for the multilevel supervision of a meshed DC microgrid. A constrained optimization-based control approach (via differential flatness, B-spline parametrization and Model Predictive Control) was presented for solving the power balancing problem minimizing, at the same time, the cost and the power dissipation. Further improvements are related to the analysis of the control scheme robustness under unexpected events, such as continuity of the system operation in case of faulted transmission lines, will be investigated.

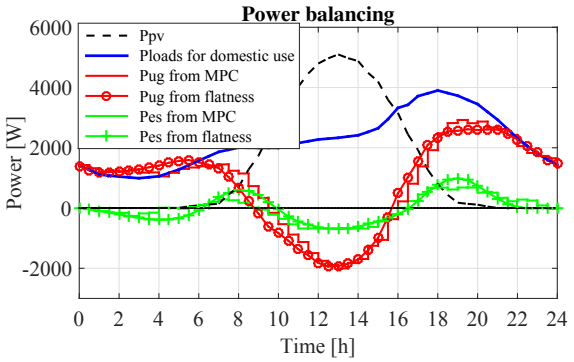

Fig. 10. Comparisons of P_{es} and P_{ug} optimal profiles obtained by flatness approach and MPC.

ACKNOWLEDGEMENTS

This work is funded by the French National Research Agency within the framework of the project ANR-15-CE05-004-02 $C^3\mu$ (Components, Control and Communication). We also acknowledge the support of the PHC Alliance project No.43234RH. Finally, we thank BUI Ngoc Thanh Hung for helping with the code implementation.

REFERENCES

Iovine, A., Siad, S.B., Damm, G., De Santis, E., and Di Benedetto, M.D. (2017). Nonlinear control of a dc microgrid for the integration of photovoltaic panels. *IEEE Transactions on automation science and engineering*, 14(2), 524–535.

Levine, J. (2009). *Analysis and control of nonlinear systems: A flatness-based approach*. Springer Science & Business Media.

Nahata, P., La Bella, A., Scattolini, R., and Ferrari-Trecate, G. (2019). Hierarchical control in islanded dc microgrids with flexible structures. *arXiv preprint arXiv:1910.05107*.

Prodan, I., Stoican, F., and Louembet, C. (2019). Necessary and sufficient LMI conditions for constraints satisfaction within a B-Spline framework. In *2019 IEEE 58th Conference on Decision and Control (CDC) December 11-13, Palais des Congrés et des Expositions Nice Acropolis, Nice, France*.

Vazquez, N., Yu, S.S., Chau, T.K., Fernando, T., and Iu, H.H.C. (2018). A fully decentralized adaptive droop optimization strategy for power loss minimization in microgrids with pv-bess. *IEEE Transactions on Energy Conversion*, 34(1), 385–395.

Velarde, P., Valverde, L., Maestre, J.M., Ocampo-Martínez, C., and Bordons, C. (2017). On the comparison of stochastic model predictive control strategies applied to a hydrogen-based microgrid. *Journal of Power Sources*, 343, 161–173.

Zafeiratou, I., Prodan, I., Lefèvre, L., and Piétrac, L. (2020). Meshed dc microgrid hierarchical control: A differential flatness approach. *Electric Power Systems Research*, 180, 106133.